materials

MDPI

Article

Unveiling the Origin of Alkali Metal (Na, K, Rb, and Cs) Promotion in CO_2 Dissociation over Mo_2C Catalysts

Renmin Liu [1,2], Congmei Chen [3], Wei Chu [1,*] and Wenjing Sun [2,*]

[1] School of Chemical Engineering, Sichuan University, Chengdu 610065, China; 17806241710@163.com
[2] China-America Cancer Research Institute, Guangdong Provincial Key Laboratory of Medical Molecular Diagnostics, Guangdong Medical University, Dongguan 523808, China
[3] National Supercomputing Center in Shenzhen (Shenzhen Cloud Computing Center), Shenzhen 518055, China; chencm@nsccsz.gov.cn
* Correspondence: chuwei1965@foxmail.com (W.C.); swj_gdmc@163.com (W.S.)

Abstract: Molybdenum carbide (Mo_2C) is a promising and low-cost catalyst for the reverse water−gas shift (RWGS) reaction. Doping the Mo_2C surface with alkali metals can improve the activity of CO_2 conversion, but the effect of these metals on CO_2 conversion to CO remains poorly understood. In this study, the energies of CO_2 dissociation and CO desorption on the Mo_2C surface in the presence of different alkali metals (Na, K, Rb, and Cs) are calculated using density functional theory (DFT). Alkali metal doping results in increasing electron density on the Mo atoms and promotes the adsorption and activation of CO_2 on Mo_2C; the dissociation barrier of CO_2 is decreased from 12.51 on Mo_2C surfaces to 9.51–11.21 Kcal/mol on alkali metal-modified Mo_2C surfaces. Energetic and electronic analyses reveal that although the alkali metals directly bond with oxygen atoms of the oxides, the reduction in the energy of CO_2 dissociation can be attributed to the increased interaction between CO/O fragments and Mo in the transition states. The abilities of four alkali metals (Na, K, Rb, and Cs) to promote CO_2 dissociation increase in the order Na (11.21 Kcal/mol) < Rb (10.54 Kcal/mol) < Cs (10.41 Kcal/mol) < K (9.51 Kcal/mol). Through electronic analysis, it is found that the increased electron density on the Mo atoms is a result of the alkali metal, and a greater negative charge on Mo results in a lower energy barrier for CO_2 dissociation.

Keywords: molybdenum carbide; alkali metal; RWGS; DFT

Citation: Liu, R.; Chen, C.; Chu, W.; Sun, W. Unveiling the Origin of Alkali Metal (Na, K, Rb, and Cs) Promotion in CO_2 Dissociation over Mo_2C Catalysts. *Materials* **2022**, *15*, 3775. https://doi.org/10.3390/ma15113775

Academic Editor: Laura Calvillo

Received: 9 April 2022
Accepted: 20 May 2022
Published: 25 May 2022

1. Introduction

Increasing atmospheric CO_2 concentrations have resulted in global warming [1–3]. Therefore, CO_2 capture, storage, and catalytic reduction have drawn attention to reduce this environmental burden [4]. In particular, the reverse water–gas shift (RWGS) reaction, which reduces CO_2 to CO as an intermediate to generate methanol or other hydrocarbons, is promising [3]. The RWGS reaction is endothermic; thus, the RWGS reaction is thermodynamically favorable at high temperatures, as shown in Equation (1) [5].

$$CO_2 + H_2 \rightarrow CO + H_2O \quad \Delta H^{\circ}_{298K} = 41 \text{ KJ/mol} \tag{1}$$

Noble metal catalysts such as Pt [6,7], Rh [8,9], and Au [10] show reasonable activity and selectivity for the RWGS reaction but are costly. However, supported noble metal catalysts frequently suffer the problem of sintering under high temperature conditions. Moreover, noble metal catalysts are relatively expensive and scarce, which limits their ability to be widely used for CO_2 hydrogenation. Transition metal carbides (TMCs) such as Mo_2C [11,12], WC [13], and TiC [14] are considered as attractive candidates for the RWGS reaction because of their low cost and similar catalytic activity to platinum-based catalysts. TMCs have good performance in the reaction of CO_2 conversion into CO [15], CH_4 [16],

CH_3OH [17], and other hydrocarbons [18,19]. Among the carbide family members, molybdenum carbide (Mo_2C) shows particularly high RWGS activity because of its favorable activity for C=O bond scission and H_2 dissociation [20].

Alkali metals are very good promoters for CO_2 conversion [21–23]. For example, CO_2 activation was accelerated in K-modified CuxO/Cu (111) catalysts due to the geometric and electronic effects introduced by K [24]. The modification of Rh/Al_2O_3 with K changes the surroundings of the Rh particles, which influences the strength of CO adsorption and the activation ability of Rh for H_2 dissociation [9]. The modification of Mo_2C with alkali metals changes the structural and electronic properties of these catalysts and promotes the performances of Mo_2C in CO_2 conversions [25–29]. For example, the addition of 2 wt% K to Mo_2C/γ-Al_2O_3 increases the CO selectivity to 95% from 73.5% [30], and the incorporation of K into Cu/Mo_2C results in high CO_2 dissociation activity (almost 1.5 times higher than Cu/Mo_2C) but also reduces H_2 adsorption, thus resulting in a low H_2/CO_x ratio and low CH_4 production [31]. The CO selectivity of Cs-Mo_2C, which can reach 100% at low-temperatures (400 to 500 °C), is a result of increased electron transfer from Cs to Mo, thus favoring CO selectivity [28]. By the introduction of K into the single atom catalyst $Rh0.2/\beta$-Mo_2C, the selectivity of hydrogenation of CO_2 to ethanol is much-improved, and the catalysts exhibit up to 72.1% of ethanol selectivity at low temperature (150 °C) [32].

Although the promotion effects of alkali metals on TMCs have been observed experimentally, the structural and electronic effects of alkali metals on TMCs in the RWGS reaction remain unknown. Additionally, different alkali metals affect the WGS and RWGS reactions to various extents. For instance, when Na and K species are introduced into WC, they both promote the improvement of the selectivity of WC for the RWGS reaction at low temperatures (300–350 °C), and the highest CO yield is achieved using K-promoted WC [13]. Kowalik et al. [33] reported that the promotional effect of alkali metals on the WGS activity of $Cu/ZnO/Al_2O_3$ catalysts increases in the order of Li < Na < K < Cs, but the promotional effects of H_2O and CO_2 dissociation induced by alkali metals increase in the order of Na < K < Rb < Cs over Cu (111) catalysts [22]. However, the reasons underlying these observations remain unknown.

In this study, we investigated the effect of the modification of the surface of Mo_2C catalysts with alkali metals (Na, K, Rb, and Cs) using density functional theory calculations and revealed the key electronic effects affecting the adsorption of the reactants and intermediate species, the desorption of the products, as well as the barrier of CO_2 dissociation. Furthermore, the energy barrier of CO_2 dissociation was correlated with the adsorption energy of surface species, thus revealing the origin of the promoting effects of various alkali metals on RWGS activity. Our findings further highlight the importance of modifying molybdenum carbide with alkali for carbon dioxide reduction.

2. Computation Detail and Models

All calculations were performed by using the $DMol^3$ code within the Materials Studio 7.0 program [34]. The generalized gradient approximation (GGA) with the Perdew–Burke–Ernzerhof (PBE) functional [35] was selected to calculate the exchange-correlation energy. The wave functions were expanded by the utilization of the double numerical quality basis set with polarization functions (DNP) [36]. The energy, gradient, and displacement convergence criteria were 1×10^{-5} hartree, 2×10^{-3} hartree/Å, and 5×10^{-3} Å, respectively.

LST/QST was used to perform the transition states (TS) search [37,38]. The convergence criterion of the TS search was set to 0.002 Ha/Å on each atom. Only one virtual frequency could be considered as the real transition state.

The adsorption energy (E_{ads}) of all intermediate species on the surface of catalyst was defined as:

$$E_{ads} = E_{tot} - E_{cat} - E_{gas} \quad (2)$$

where E_{tot} is the total energy of the adsorbed species on the catalyst, E_{cat} is the total energy of the clean catalyst, and E_{gas} is the energy of the molecules in the gas phase. The activation barrier ($E_{Barrier}$) and reaction energy (ΔE) were calculated using the formulas:

$$E_{Barrier} = E_{TS} - E_{IS} \quad (3)$$

$$\Delta E = E_{FS} - E_{IS} \quad (4)$$

Here, E_{IS}, E_{TS}, and E_{FS} represent the total energies of the initial state (IS), transition state (TS), and the final state (FS), respectively.

By applying geometry optimizations based on the minimization of the total energy of the unit cell, the DFT lattice parameters were found to be a = 6.00 Å, b = 5.78 Å, and c = 4.71 Å, which were in good agreement with the experimental results [39]. The slab model of the β-Mo_2C (001) surface contained six atomic layers with a total of 24 C atoms and 48 Mo atoms in one unit cell (using a 2 × 2 supercell with size 12.00 × 11.57 × 4.71 Å, with a vacuum space of 20 Å). During the structural optimization, the bottom two layers were constrained in their bulk positions, whereas all the other atoms were allowed to relax. For alkali metal-modified β-Mo_2C (001), one alkali atom (Na, K, Rb, Cs) was placed at different sites of the top layer of the molybdenum layer. After geometry optimization, the site that exhibited the strongest binding to K atom was selected for further calculations.

3. Results and Discussion

3.1. Optimized Structure of Alkali-Metal-Modified β-Mo_2C (001)

The four alkali metal atoms at optimized structures of the X-Mo_2C (X = Na, K, Rb, Cs) surfaces were all located on the 4F sites on the Mo_2C surface, that is, between four Mo atoms (Figure 1). The alkali metal-promoted surfaces are shown in Figure 2a–d, and the key structural parameters of the X-Mo_2C are listed in Table S1. The distances between alkali metals and Mo atoms increased with the increases in the atomic radii of the alkali metals: 3.26, 3.72, 3.89, and 4.04 Å on average for Na, K, Rb, and Cs, respectively. In addition, after the addition of the alkali metal, the Mo_1–Mo_3 and Mo_3–M_4 bonds increased in length by 0.04–0.06 Å, whereas the Mo_1–Mo_4 bond length was shortened by 0.03 Å for all X-Mo_2C. The coverage of alkali metals on X-Mo_2C surfaces was a 0.014 mono layer.

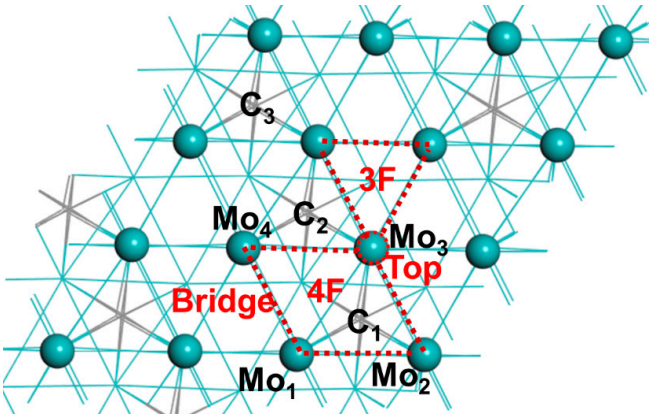

Figure 1. Position of the selected adsorption sites for alkali metal atoms. Color codes: Mo—green, carbon—grey, the first surface layer is shown using the ball and stick model, and the last five layers are shown using the line model.

As shown by the charge analysis in Table 1, the Mulliken charge on Mo atoms in bare Mo_2C was positive. In contrast, after the addition of the alkali metal, the charge on the adjacent Mo atoms became negative, suggesting the transfer of electrons from the alkali metal to Mo. Moreover, the closest Mo atoms to the alkali metal gained the most electrons. Because Rb and Cs atoms are less electronegative than the other alkali metals, they increased

the electron density of the surface Mo atoms and subsurface C atoms. Therefore, in Rb- and Cs-Mo_2C, the charges on Mo atoms were less negative than those of K and Na-Mo_2C.

In addition, we calculated the changes in the d-band center [40] as a result of charge transfer between Mo and alkali metal atoms (Figure 2e). The d-band center before and after the addition of the alkali metal remained the same, consistent with previous findings [41,42].

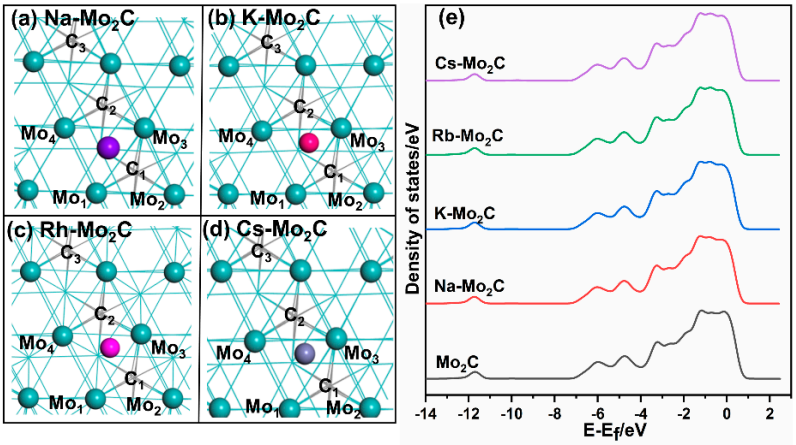

Figure 2. The most stable structure of X−Mo_2C (001): (**a**) Na−Mo_2C, (**b**) K−Mo_2C, (**c**) Rb−Mo_2C, and (**d**) Cs−Mo_2C; (**e**) d−band center of Mo atoms on Mo_2C and X-Mo_2C (X = Na, K, Rb, and Cs). Color codes: Mo—green, carbon—grey (shown in line model).

Table 1. Mulliken charges (*e*) of key atoms in the clean and X-Mo_2C (X = Na, K, Rb, Cs) *.

Catalysts	Mulliken Charge (*e*)						
	X	Mo_1	Mo_3	Mo_4	C_1	C_2	C_3
Mo_2C	/	0.05	0.05	0.13	−0.50	−0.50	−0.50
Na-Mo_2C	0.55	−0.08	−0.09	0.02	−0.47	−0.46	−0.45
K-Mo_2C	0.72	−0.10	−0.09	0.03	−0.52	−0.51	−0.49
Rb-Mo_2C	0.65	−0.06	−0.05	0.10	−0.61	−0.60	−0.60
Cs-Mo_2C	0.66	−0.07	−0.06	0.09	−0.54	−0.53	−0.53

* Atom labels are indicated in Figure 1.

3.2. Adsorption of Intermediate Species on Mo_2C and X-Mo_2C Surfaces

The schematic mechanism of the redox pathway is shown in Figure 3. We calculated the adsorption energy (E_{ads}) and key parameters of CO_2, CO, and O* species on bare and X-Mo_2C surfaces involved in the redox pathway (shown in Figure 4 and Table S2).

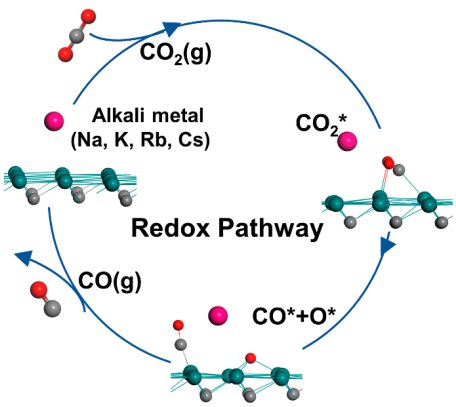

Figure 3. Schematic mechanism diagram of redox pathway in the RWGS reaction. The species with asterisks (*) represent adsorbed species.

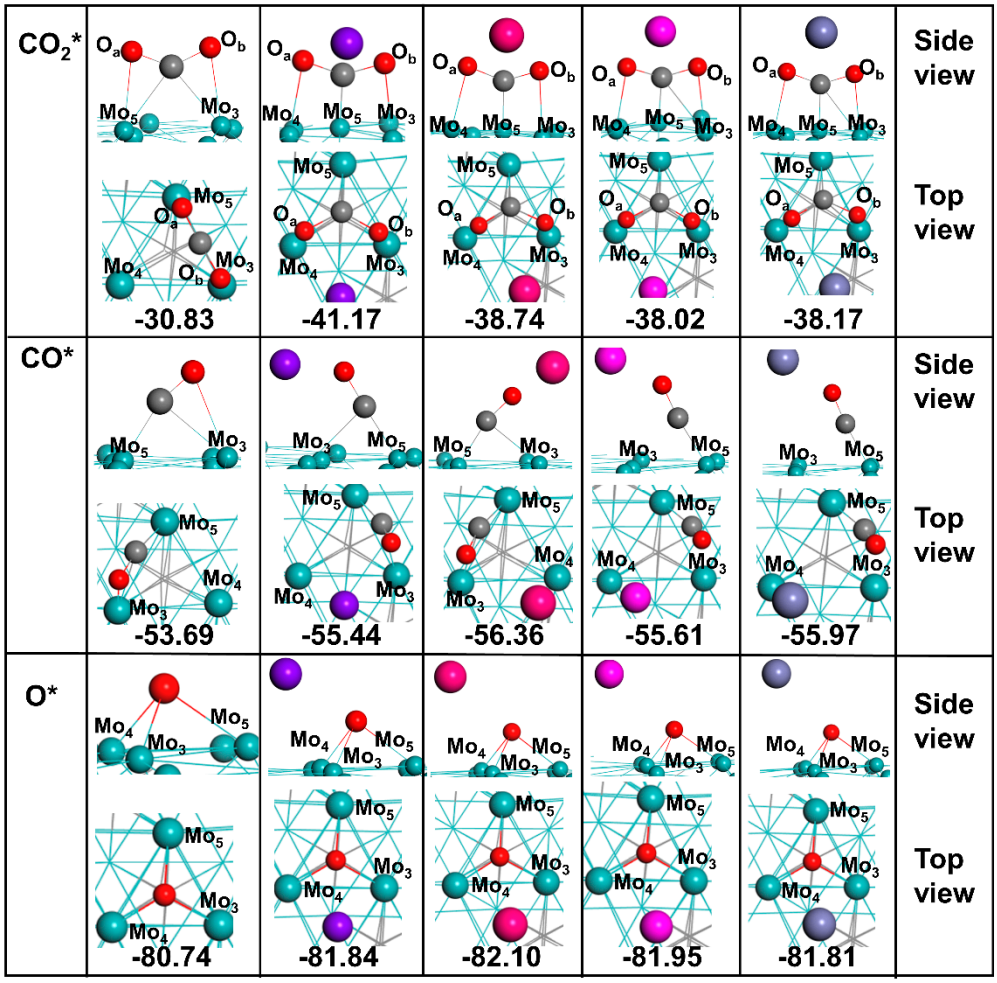

Figure 4. The most stable adsorption configurations of all possible surface intermediates as well as the adsorption energies (in Kcal/mol) on Mo_2C and X−Mo_2C (X = Na, K, Rb, and Cs). The species with asterisks (*) represent adsorbed species. Color codes: Mo—green, carbon—grey, O—red.

3.2.1. Adsorption of CO_2*

The most stable adsorption configuration of CO_2 on Mo_2C is shown in Figure 4, having an adsorption energy of −30.83 Kcal/mol, consistent with the literature value [30]. The C atom in CO_2 was positioned at the bridge site between Mo_3 and Mo_5, and the two C–Mo bonds were 2.24 Å in length. The nearest distance between the O and Mo atoms was 2.12 Å for O_a–Mo_3 and 2.43 Å for O_b–Mo_5. The interaction of CO_2 with Mo_2C led to the elongation of the C–O bonds from 1.17 Å in the vacuum calculations to 1.26 Å in the adsorbed molecule, and the bond angle increased to 135°.

For the adsorption of CO_2 on all X-Mo_2C surfaces, the carbon atom of CO_2 was attached to the top site of one Mo atom, and the oxygen atoms formed two Mo–O bonds with the adjacent Mo atoms. The E_{ads} of CO_2 was −41.17 Kcal/mol on Na-Mo_2C, −38.74 Kcal/mol on K-Mo_2C, −38.02 Kcal/mol on Rb-Mo_2C, and −38.17 Kcal/mol on Cs-Mo_2C. For CO_2 adsorption on Na-Mo_2C, the two O atoms in CO_2 were equidistant from the Na atom (2.41 Å), CO_2 was bent to 114°, and the C–O bonds were elongated to 2.41 Å. For the K-Mo_2C catalyst, the K … O_a and K … O_b distances were found to be 2.74 and 2.97 Å, respectively, the CO_2 bond was 115.6°, and the O–C bonds were elongated to 1.35 and 1.34 Å. For Rb-Mo_2C, the Rb … O distances were 3.08 and 2.96 Å, and the C–O_a and C–O_b bond lengths were stretched to 1.34 and 1.36 Å, respectively. For Cs-Mo_2, the Cs … O_a and Cs … O_b distances were 3.06 and 3.16 Å, respectively. Moreover, the C–O_a and C–O_b bond lengths were 1.33 and 1.36 Å, respectively.

Thus, the X–O distances were close to the sum of the X^+ and O^{2-} atomic radii, namely 2.41 Å for $Na^+ + O^{2-}$, 2.77 Å for $K^+ + O^{2-}$, 2.91 Å for $Rb^+ + O^{2-}$, and 3.06 for $Cs^+ + O^{2-}$, as also observed for the X–O distances in crystalline metal oxides, for example, 2.40 Å in Na_2O [43], 2.79 in K_2O [43], 2.92 in Rb_2O [43], and 3.26 Å in CsO_2 [44]. These findings indicate that the electrostatic interaction between O and X was strong and similar to the ionic bonding between O and X in X_2O. Wang et al. found that for oxygenate species adsorbed on K^+-modified Cu (111) and Cu (110) surfaces, when the distance between K and O atoms was 3.00 Å, direct bonding between $O^{\delta-}$ and $K^{\delta+}$ ions occurred [22]. Further, a short distance between X and O generated a longer C–O bond, indicating that stronger X–O interactions promote CO_2 activation. Therefore, alkali metals could promote the adsorption and activation of CO_2, consistent with theoretical and experimental findings [30].

Our charge analysis (Table S3) suggested that electrons are transferred from the alkali metal to Mo atoms and, thus, affect the surface charge of Mo_2C [28]. Therefore, when CO_2 was adsorbed on Mo_2C, the Mo atoms lost electrons and CO_2 gained 0.29 *e*. In contrast, when CO_2 was adsorbed on X-Mo_2C, the Mo atoms became more positive (lost more electrons); for example, CO_2 gained 0.74 *e* on Na-Mo_2C, 0.71 *e* on K-Mo_2C, 0.73 *e* on Rb-Mo_2C, and 0.69 *e* on Cs-Mo_2C. The increase in the charge of CO_2 also indicated enhanced charge transfer via alkali metal promotion. Moreover, in the X-Mo_2C surfaces, alkali metal atoms lost electrons by 0.72 *e* for Na, 0.82 *e* for K, 0.76 *e* for Rb, and 0.74 *e* for Cs, respectively. Therefore, on one hand, alkali metal atoms donated electrons to CO_2, but, on the other hand, they facilitated electron transfer from Mo to CO_2 and thus promoted CO_2 activation.

3.2.2. Adsorption of CO*

When CO adsorbed on the Mo_2C surface, the carbon atom of CO_2 was adsorbed on the bridge sites between Mo_3 and Mo_5 with an orientation tilted toward Mo_4. The generated C–Mo_4, C–Mo_5, and O–Mo_4 bond lengths were 2.27, 1.99, and 2.35 Å, respectively. Further, the C–O bond length was elongated to 1.23 Å, and the E_{ads} of CO on Mo_2C was −53.69 Kcal/mol.

The E_{ads} values of CO on X-Mo_2C (X = Na, K, Rb, and Cs) were around −56 Kcal/mol, approximately 1.75–2.67 Kcal/mol greater than that on Mo_2C. The maximum differences in E_{ads} on the X-Mo_2C surfaces were within 1 Kcal/mol, i.e., negligible. In these systems, CO was adsorbed in a tilted orientation on the bridge sites of Mo_3–Mo_5 atoms with the oxygen atom oriented towards the Mo_3 atom. The distances between alkali metal and O (in CO) were 2.42 Å for Na ... O, 2.78Å for K ... O, 2.93 Å for Rb ... O, and 3.18 Å for Cs ... O, suggesting that the alkali metals formed direct bonds with the O atom in CO in X-Mo_2C systems. The Mulliken charge analysis (Table S4) showed that more electrons transferred to CO on X-Mo_2C than that on bare Mo_2C. Therefore, the addition of alkali metal atoms increased the adsorption of CO as compared with the clean surface and resulted in longer C–O bonds.

3.2.3. Adsorption of O*

Atomic oxygen adsorbed on the 3F sites between the Mo_3–Mo_4–Mo_5 atoms, having average Mo–O bond lengths of 2.08 Å and E_{ads} of −80.74 Kcal/mol. The E_{ads} for O* on the surface of X-Mo_2C (X = Na, K, Rb, and Cs) ranged from −81.64 to −82.10 Kcal/mol, slightly greater than that on bare Mo_2C. The average distances between O* and Mo_3 atoms were 2.46 Å for Na, 2.85Å for K, 3.03 Å for Rb, and 3.04 Å for Cs. On bare Mo_2C, the atomic oxygen gained 0.66 *e* from the surface of Mo atoms, whereas for X-Mo_2C, the O atom gained more electrons, namely 0.74 *e* from Na-Mo_2C, 0.73 *e* from K-Mo_2C, 0.72 *e* from Rb-Mo_2C, and 0.73 *e* from Cs-Mo_2C (see Table S5). Moreover, the Mo atoms in the X-Mo_2C surfaces were more positive, suggesting that the addition of alkali metals promoted the loss of electrons from the Mo atoms around O*.

3.3. Energy Barriers for CO_2 Dissociation on Mo_2C and Alkali-Metal-Modified Mo_2C Surfaces

Currently, the RWGS reaction mechanisms are classified into redox- (or direct-), carboxyl-, and formate-mediated routes. Chen et al. [45] performed ambient-pressure X-ray photoelectron spectroscopy (AP-XPS) measurements on the Mo_2C catalyst, and they did not find intermediate species (carbonate, formate, carbonyl, etc.) under reaction conditions. Furthermore, they proved that CO_2 was directly dissociated on Mo_2C to produce CO and oxycarbide (Mo_2C-O). Surface oxygen (Mo_2C-O) was removed subsequently by hydrogen to produce H_2O to complete the catalytic cycle [46]. Moreover, the elemental steps for CO_2 dissociation to CO* and O* are known to be the rate limiting steps on both bare Mo_2C and K-modified Mo_2C catalysts [30]. Thus, the activation barriers for CO_2 dissociation on the various alkali metal-modified Mo_2C surfaces were studied and compared.

In Figure 5, we show the activation energy profiles of CO_2 dissociation on the (a) bare, (b) Na-promoted, (c) K-promoted, (d) Rb-promoted, and (e) Cs-promoted Mo_2C (001) surfaces. The activation barrier for CO_2 dissociation on Mo_2C surfaces was found to be 12.51 Kcal/mol, and the O–CO bond lengths of the transition states (TSs) were found to be 1.75 Å, indicating the cleavage of a C–O bond. The activation energies for this reaction were remarkably different on the four X-Mo_2C surfaces, namely 11.21 Kcal/mol for Na-Mo_2C, 9.51 Kcal/mol for K-Mo_2C, 10.54 Kcal/mol for Rb-Mo_2C, and 10.41 Kcal/mol for Cs-Mo_2C, lower than that on bare Mo_2C. For CO_2 dissociation on the X-Mo_2C surfaces, the bond length of C–O_b was elongated, ranging from 1.81 to 1.87 Å in the TS, respectively, longer than that on bare Mo_2C. In addition, the distance between Na, K, Rb, and Cs and O_a in CO_2 were 2.14, 2.94, 3.07, and 3.06 Å, respectively, suggesting the interaction between X and O throughout the reaction and suggesting the key role of the alkali metal in CO_2 dissociation, consistent with experimental observations [47–49].

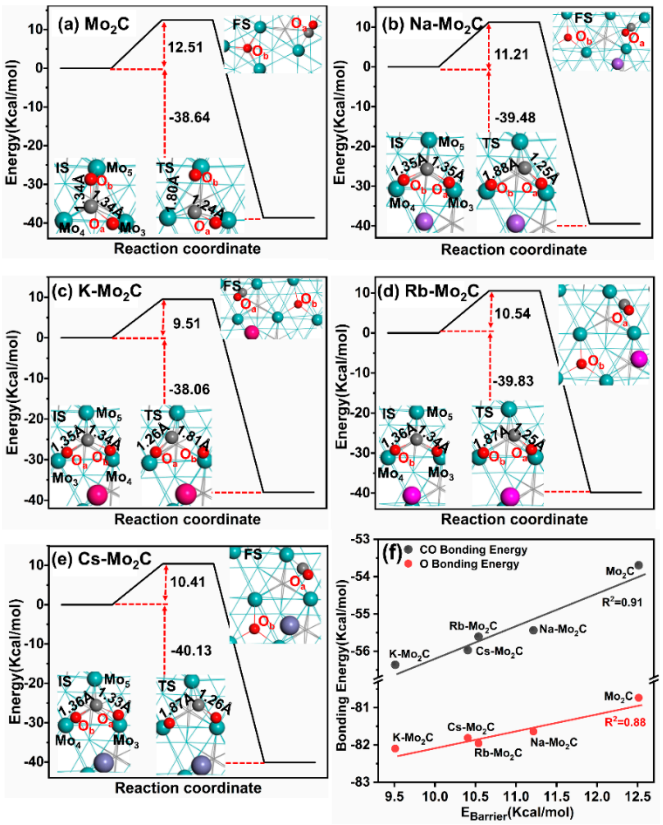

Figure 5. CO_2 dissociation profiles on (**a**) Mo_2C, (**b**) Na−Mo_2C, (**c**) K−Mo_2C, (**d**) Rb−Mo_2C, and (**e**) Cs−Mo_2C. (**f**) Correlation between activation energy of the CO_2 dissociation and CO/O bonding energy.

Figure 5 suggests that the transition state for CO_2 dissociation is a late (product-like) transition state. Therefore, for CO_2 dissociation, the stabilization of the final state should also stabilize the transition state, resulting in a lower activation barrier. Figure 5f shows that the CO_2 dissociation barrier was strongly influenced by the E_{ads} of CO and O fragments on the catalyst surfaces, and stronger CO or O binding resulted in lower CO_2 dissociation barriers. Therefore, the identification of the role of the alkali metal atom on the stability of adsorbed CO and O during the reaction is necessary.

3.4. Energetic Analysis

As discussed earlier, alkali metals enhance the RWGS activity of Mo_2C by decreasing the energy barriers for CO_2 dissociation. Thus, to elucidate the effects of the alkali metals, the physical origin of the reaction barriers for CO_2 dissociation on both bare and X-Mo_2C surfaces were assessed using energy decomposition, as proposed by Hammer [50,51] (Equation (4)), and the results are listed in Table 2.

$$E_{Barrier} = E_{bond}^{CO_2} - E_{CO_2}^{IS} + E_{CO}^{TS} + E_{O}^{TS} + E_{int}^{TS} \quad (5)$$

where $E_{bond}^{CO_2}$ represents the bonding energy of CO_2 in gas. $E_{CO_2}^{IS}$, E_{CO}^{TS}, E_{O}^{TS}, and E_{int}^{TS} refer to binding energy of CO_2* in the IS, binding energy of CO* (O*) in the TS, and the interaction of CO with O in the TS, respectively.

Table 2. Energy decomposition of the calculated activation barriers for the dissociation of CO_2 on bare Mo_2C and X-Mo_2C.

Catalysts	$E_{Barrier}$	$E_{CO_2}^{IS}$	E_{CO}^{TS}	E_{O}^{TS}	E_{int}^{TS}	$E_{int}^{CO\text{-}X}$ [a]	$E_{int}^{CO\text{-}Mo}$	$E_{int}^{O\text{-}X}$ [a]	$E_{int}^{O\text{-}Mo}$	ΔE_{CO}^{TS} [b]	ΔE_{O}^{TS} [b]
Mo_2C	12.45	−50.78	−44.89	−72.33	−68.64	0.00	−44.89	0.00	−72.33	0.00	0.00
Na-Mo_2C	11.30	−60.28	−47.39	−74.22	−75.04	−0.09	−47.29	−0.28	−73.94	−2.50	−1.89
K-Mo_2C	9.45	−60.44	−51.82	−73.31	−73.38	−0.12	−51.71	−0.32	−73.00	−6.93	0.99
Rb-Mo_2C	10.61	−61.34	−47.14	−75.08	−76.17	−0.12	−47.03	−0.25	−74.82	−2.25	−2.75
Cs-Mo_2C	10.38	−60.11	−45.36	−76.04	−75.89	−5.77	−45.32	−0.25	−75.77	−0.47	−3.71

[a] The interaction energies of A-X as well as between A and Mo atoms at the TSs (A refers to adsorption species). The C−O bonding energy of CO_2 in the gas phase is calculated to be 147.59 Kcal/mol. [b] $\Delta E_A^{TS} = E_{A,\,X-Mo_2C}^{TS} - E_{A,\,Mo_2C}^{TS}$.

In the C–O bond scission of CO_2 on Mo_2C surfaces, alkali metals stabilize the binding of CO_2 in the IS, which is unfavorable for reducing the energy barrier (Table 2). However, by strengthening CO and O binding in the TS (E_{CO}^{TS} and E_{O}^{TS}) on X-Mo_2C relative to those on clean surfaces, the alkali metal reduces the energy barrier and promote CO_2 dissociation. In addition, all alkali metals can enhance the stability of CO or O fragments in the TS on Mo_2C. However, Na- and K-modified surfaces effectively stabilize adsorbed CO compared to bare Mo_2C $\left(\Delta E_{CO}^{TS} > \Delta E_{O}^{TS}\right)$, whereas Rb- and Cs-modified surfaces stabilize adsorbed O $\left(\Delta E_{O}^{TS} > \Delta E_{CO}^{TS}\right)$. Therefore, $Max\Delta E_S^{TS}$, i.e., the maximum of ΔE_{CO}^{TS} and ΔE_{O}^{TS} was plotted against the energy barrier for CO_2 dissociation. Figure 6 shows that the energy barrier for CO_2 dissociation on X-Mo_2C was linearly correlated to $Max\Delta E_S^{TS}$ (R^2 = 0.90), and a greater value of $Max\Delta E_S^{TS}$ indicated a larger decrease of the barrier and a stronger promoting effect of the alkali metal. In other words, increasing the E_{ads} of the CO and O fragments in the TS can effectively reduce the energy barrier, but the extent of the barrier reduction depends on the balance of stabilities of adsorbed CO and O resulting from alkali metal addition.

As displayed in Figure 5, the alkali metals interacted with CO and O on the X-Mo_2C surfaces throughout the reaction. Hence, apart from the interaction between these adsorbates and surface Mo atoms, the interaction between them and the alkali metal adatom also made up the interaction of them with X-Mo_2C.The interaction energies of the interactions

between adsorbates and alkali metals were calculated with the following formulas, and the results are listed in Table 3.

$$E_{int}^{A-X} = E_{A/X}^{TS} - (E_A + Ex - E_{surf}^{TS}) \quad (6)$$

$$E_{int}^{A-Mo} = E_A^{TS} - E_{int}^{A-X} \quad (7)$$

$E_{A/X}^{TS}$, E_A, and Ex represent the energies of the A−alkali metal complex, isolated A, and alkali metal at Mo_2C surfaces, respectively; and E_{surf}^{TS} refers to the energy of the clean surface at the TS.

As shown in Table 3, the addition of alkali metal adatoms resulted in interactions between the alkali metal and oxygen species in the TS, but there was little correlation between $E_{int}^{CO-X}/E_{int}^{O-X}$ and $E_{Barrier}$. However, the addition of alkali metals increased the strength of the O−Mo or CO–Mo bonds, as shown by the greater E_{int}^{CO-Mo} and E_{int}^{O-Mo} on X-Mo_2C compared to those on bare Mo_2C. In addition, the increase in the CO–Mo and O–Mo interactions in X-Mo_2C (E_{int}^{CO-Mo} and E_{int}^{O-Mo}) was linearly related to the increase in the bonding energies of CO (ΔE_{CO}^{TS}) and O (ΔE_{O}^{TS}) in the TS. Therefore, the increased bonding energies of CO and O in the TS were a result of the increased Mo–O and Mo–CO bond strength resulting from the addition of alkali metals.

Previous studies have demonstrated that the activation of CO_2 requires electron transfer from the catalyst to CO_2 [52–55]. The charge analysis in Table 3 shows that the enhancement in the Mo–O and Mo–CO interactions was due to the addition of alkali metals, which induced the accumulation of electron density at Mo and, thus, electron transfer from Mo to CO and O in the TS. Further, we observed a linear increase in the negative charge on the Mo atoms (increase in electron density) in the Na, Rb, Cs, and K-Mo_2C surfaces, which was consistent with the reduction in $E_{Barrier}$. This result indicated that the increase in charge at Mo resulted in a lower $E_{Barrier}$. Additionally, although Rb and Cs are less electronegative than the other alkali metals, they transferred electrons to both Mo and C in the subsurface; thus, fewer electrons accumulated at Mo in Rb/Cs-Mo_2C than in K-Mo_2C.

In summary, the CO_2 dissociation energy barrier was in the order of Mo_2C (12.45 Kcal/mol) > Na (11.21 Kcal/mol) > Rb (10.54 Kcal/mol) > Cs (10.41 Kcal/mol) > K(9.51 Kcal/mol). This is because the K atom promoted the most electrons accumulated at the Mo atom and thereby generated the strongest Mo–CO interactions in the TS. The significantly improved stability of CO fragments in the TS led to the energy barrier of CO_2 dissociation on K-Mo_2C being the lowest.

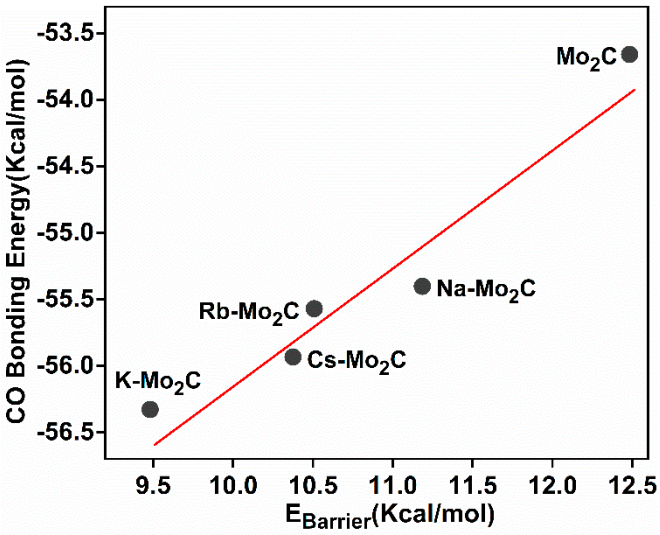

Figure 6. Correlation between activation energy of the CO_2 dissociation and $Max\Delta E_S^{TS}$ (fitting model: $y = 2.16x - 26.56$; $R^2 = 0.90$).

Table 3. Mulliken charges (*e*) of key atoms in the calculated transition states.

	Mo		CO_2			
	Mo_1 [a]	Mo_2 [b]	O_a	C	O_b	Alkali Metal
Mo_2C	0.19	0.30	−0.30	0.15	−0.50	
Na-Mo_2C	0.12	0.17	−0.41	0.19	−0.61	0.74
K-Mo_2C	0.06	0.23	−0.42	0.16	−0.60	0.83
Rb-Mo_2C	0.20	0.19	−0.39	0.13	−0.58	0.77
Cs-Mo_2C	0.18	0.18	−0.40	0.18	−0.59	0.76

[a] Mo atom that bonded with O_a, [b] Mo atom that bonded with O_b.

3.5. CO Desorption on Mo_2C and Alkali-Metal-Modified Mo_2C Surfaces

Next, we calculated the energies of CO desorption on the surfaces of bare Mo_2C and X-Mo_2C (Figure 7). The CO desorption energy on bare Mo_2C was endothermic by 63.65 Kcal/mol. The addition of alkali metals on Mo_2C slightly increased the difficulty of CO desorption. Mpourmpakis et al. found that by pre-adsorption of low-coverage oxygen (<0.50 ML), the desorption of CO on K-modified Mo_2C could be effectively promoted [56].

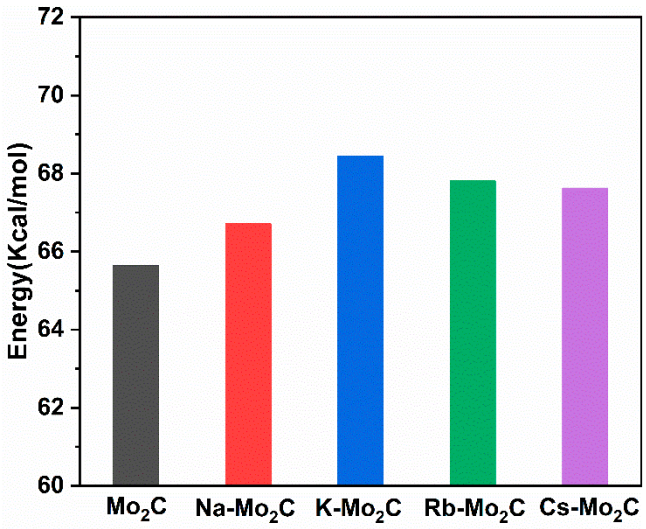

Figure 7. The desorption energy of CO on bare and X-Mo_2C, where X = Na, K, Rb, Cs.

4. Conclusions

The activity of CO_2 dissociation into CO on bare Mo_2C and those on promoted surfaces of X-Mo_2C (X = Na, K, Rb, and Cs) were studied using DFT calculations. The addition of alkali metal elements induced the accumulation of negative charges on the Mo atoms and thus promoted the adsorption and activation of CO_2 on Mo_2C. The CO_2 dissociation energy barrier was in the order of Mo_2C (12.45 Kcal/mol) > Na (11.21 Kcal/mol) > Rb (10.54 Kcal/mol) > Cs (10.41 Kcal/mol) > K (9.51 Kcal/mol). On the basis of energetic and electronic analysis, although the alkali metals directly bonded with oxygen atoms in the adsorbed oxygen species, the main reason for the reduction in the energy of CO_2 dissociation was the stronger interaction between CO/O fragments and Mo in the TS. Through electronic analysis, the promoting effects of alkali metals were influenced by the difference in the increase of electron density at the Mo atoms. Specifically, the greater the negative charge on the Mo site, the lower the energy barrier for CO_2 dissociation. In comparison, the K atom promoted the most electrons accumulated at the Mo atom and thereby generated the strongest Mo–CO interactions in the TS. The significantly improved stability of CO fragments in the TS led to the energy barrier of CO_2 dissociation on K-Mo_2C being the lowest.

Supplementary Materials: The following supporting information can be downloaded at: https://www.mdpi.com/article/10.3390/ma15113775/s1, Table S1: The key structural parameters of Mo_2C and X-Mo_2C; Table S2: Adsorption energies (Kcal/mol) and bond length (Å) of all possible intermediates on the X (Na, K, Rb, Cs)-Mo_2C catalysts; Table S3: Mulliken charge; Table S4: Mulliken charge (*e*) of CO*-X-Mo_2C; Table S5: Mulliken charge (*e*) of O*-X-Mo_2C.

Author Contributions: Investigation, formal analysis and writing—original draft preparation, R.L.; Resources, software, C.C.; Formal analysis, investigation, writing-review-editing, W.C. Formal analysis, investigation, writing-review-editing, W.S. All authors have read and agreed to the published version of the manuscript.

Funding: This research was supported by the Foundation of the State Key Laboratory of High-Efficiency Utilization of Coal and Green Chemical Engineering (2019-KF-09) and the Guangdong Basic and Applied Basic Research Foundation (2020A1515010490).

Institutional Review Board Statement: Not applicable.

Informed Consent Statement: Not applicable.

Data Availability Statement: The data presented in this study are available from the corresponding author, upon reasonable request.

Conflicts of Interest: The authors declare no conflict of interest.

References

1. Pan, Y.-X.; Liu, C.-J.; Ge, Q. Effect of surface hydroxyls on selective CO_2 hydrogenation over Ni_4/γ-Al_2O_3: A density functional theory study. *J. Catal.* **2010**, *272*, 227–234. [CrossRef]
2. Liu, C.; Liu, P. Mechanistic study of methanol synthesis from CO_2 and H_2 on a modified model Mo_6S_8 cluster. *ACS Catal.* **2015**, *5*, 1004–1012. [CrossRef]
3. Wang, J.; Liu, C.-Y.; Senftle, T.P.; Zhu, J.; Zhang, G.; Guo, X.; Song, C. Variation in the In_2O_3 crystal phase alters catalytic performance toward the reverse water gas shift reaction. *ACS Catal.* **2019**, *10*, 3264–3273. [CrossRef]
4. Aresta, M.; Dibenedetto, A.; Angelini, A. Catalysis for the Valorization of Exhaust Carbon: From CO_2 to Chemicals, Materials, and Fuels. Technological Use of CO_2. *Chem. Rev.* **2014**, *114*, 1709–1742. [CrossRef]
5. Daza, Y.A.; Kuhn, J.N. CO_2 conversion by reverse water gas shift catalysis: Comparison of catalysts, mechanisms and their consequences for CO_2 conversion to liquid fuels. *RSC Adv.* **2016**, *6*, 49675–49691. [CrossRef]
6. Zhao, Z.; Wang, M.; Ma, P.; Zheng, Y.; Chen, J.; Li, H.; Zhang, X.; Zheng, K.; Kuang, Q.; Xie, Z.-X. Atomically dispersed Pt/CeO_2 catalyst with superior CO selectivity in reverse water gas shift reaction. *Appl. Catal. B Environ.* **2021**, *291*, 120101. [CrossRef]
7. Kattel, S.; Yan, B.; Chen, J.G.; Liu, P. CO_2 hydrogenation on Pt, Pt/SiO_2 and Pt/TiO_2: Importance of synergy between Pt and oxide support. *J. Catal.* **2016**, *343*, 115–126. [CrossRef]
8. Tang, Y.; Asokan, C.; Xu, M.; Graham, G.W.; Pan, X.; Christopher, P.; Li, J.; Sautet, P. Rh single atoms on TiO_2 dynamically respond to reaction conditions by adapting their site. *Nat. Commun.* **2019**, *10*, 4488. [CrossRef]
9. Heyl, D.; Rodemerck, U.; Bentrup, U. Mechanistic study of low-temperature CO_2 hydrogenation over modified Rh/Al_2O_3 catalysts. *ACS Catal.* **2016**, *6*, 6275–6284. [CrossRef]
10. Aitbekova, A.; Wu, L.; Wrasman, C.J.; Boubnov, A.; Hoffman, A.S.; Goodman, E.D.; Bare, S.R.; Cargnello, M. Low-temperature restructuring of CeO_2-supported Ru nanoparticles determines selectivity in CO_2 catalytic reduction. *J. Am. Chem. Soc.* **2018**, *140*, 13736–13745. [CrossRef]
11. Gao, J.; Wu, Y.; Jia, C.; Zhong, Z.; Gao, F.; Yang, Y.; Liu, B. Controllable synthesis of α-MoC_{1-x} and β-Mo_2C nanowires for highly selective CO_2 reduction to CO. *Catal. Commun.* **2016**, *84*, 147–150. [CrossRef]
12. Zhang, X.; Zhu, X.; Lin, L.; Yao, S.; Zhang, M.; Liu, X.; Wang, X.; Li, Y.-W.; Shi, C.; Ma, D. Highly dispersed copper over β-Mo_2C as an efficient and stable catalyst for the reverse water gas shift (RWGS) reaction. *ACS Catal.* **2016**, *7*, 912–918. [CrossRef]
13. Morse, J.R.; Juneau, M.; Baldwin, J.W.; Porosoff, M.D.; Willauer, H.D. Alkali promoted tungsten carbide as a selective catalyst for the reverse water gas shift reaction. *J. CO_2 Util.* **2020**, *35*, 38–46. [CrossRef]
14. Rodriguez, J.A.; Evans, J.; Feria, L.; Vidal, A.B.; Liu, P.; Nakamura, K.; Illas, F. CO_2 hydrogenation on Au/TiC, Cu/TiC, and Ni/TiC catalysts: Production of CO, methanol, and methane. *J. Catal.* **2013**, *307*, 162–169. [CrossRef]
15. Liu, X.; Kunkel, C.; Ramírez de la Piscina, P.; Homs, N.; Viñes, F.; Illas, F. Effective and highly selective CO generation from CO_2 using a polycrystalline α-Mo_2C catalyst. *ACS Catal.* **2017**, *7*, 4323–4335. [CrossRef]
16. Xu, W.; Ramírez, P.J.; Stacchiola, D.; Brito, J.L.; Rodriguez, J.A. The Carburization of Transition Metal Molybdates (M_xMoO_4, M=Cu, Ni or Co) and the Generation of Highly Active Metal/Carbide Catalysts for CO_2 Hydrogenation. *Catal. Lett.* **2015**, *145*, 1365–1373. [CrossRef]

17. Posada-Pérez, S.; Ramírez, P.J.; Gutiérrez, R.A.; Stacchiola, D.J.; Viñes, F.; Liu, P.; Illas, F.; Rodriguez, J.A. The conversion of CO_2 to methanol on orthorhombic β-Mo_2C and Cu/β-Mo_2C catalysts: Mechanism for admetal induced change in the selectivity and activity. *Catal. Sci. Technol.* **2016**, *6*, 6766–6777. [CrossRef]
18. Li, N.; Chen, X.; Ong, W.-J.; MacFarlane, D.R.; Zhao, X.; Cheetham, A.K.; Sun, C. Understanding of Electrochemical Mechanisms for CO_2 Capture and Conversion into Hydrocarbon Fuels in Transition-Metal Carbides (MXenes). *ACS Nano* **2017**, *11*, 10825–10833. [CrossRef]
19. Shi, Z.; Yang, H.; Gao, P.; Chen, X.; Liu, H.; Zhong, L.; Wang, H.; Wei, W.; Sun, Y. Effect of alkali metals on the performance of CoCu/TiO_2 catalysts for CO_2 hydrogenation to long-chain hydrocarbons. *Chin. J. Catal.* **2018**, *39*, 1294–1302. [CrossRef]
20. Posada-Pérez, S.; Viñes, F.; Ramirez, P.J.; Vidal, A.B.; Rodriguez, J.A.; Illas, F. The bending machine: CO_2 activation and hydrogenation on δ-MoC(001) and β-Mo_2C(001) surfaces. *Phys. Chem. Chem. Phys.* **2014**, *16*, 14912–14921. [CrossRef]
21. Yang, X.; Su, X.; Chen, X.; Duan, H.; Liang, B.; Liu, Q.; Liu, X.; Ren, Y.; Huang, Y.; Zhang, T. Promotion effects of potassium on the activity and selectivity of Pt/zeolite catalysts for reverse water gas shift reaction. *Appl. Catal. B Environ.* **2017**, *216*, 95–105. [CrossRef]
22. Wang, Y.-X.; Wang, G.-C. A systematic theoretical study of water gas shift reaction on Cu(111) and Cu(110): Potassium effect. *ACS Catal.* **2019**, *9*, 2261–2274. [CrossRef]
23. Wang, Y.-X.; Zhang, H.-L.; An, P.; Wu, H.-S.; Jia, J.-F. Effect of Potassium on Methanol Steam Reforming on the Cu(111) and Cu(110) Surfaces: A DFT Study. *J. Phys. Chem. C* **2021**, *125*, 20905–20918. [CrossRef]
24. An, W.; Xu, F.; Stacchiola, D.; Liu, P. Potassium-Induced Effect on the Structure and Chemical Activity of the CuxO/Cu(1 1 1) ($x \leq 2$) Surface: A Combined Scanning Tunneling Microscopy and Density Functional Theory Study. *ChemCatChem* **2015**, *7*, 3865–3872. [CrossRef]
25. Feng, Z.; Su, G.; Ding, H.; Ma, Y.; Li, Y.; Tang, Y.; Dai, X. Atomic alkali metal anchoring on graphdiyne as single-atom catalysts for capture and conversion of CO_2 to HCOOH. *Mol. Catal.* **2020**, *494*, 111142. [CrossRef]
26. Gao, M.; Zhang, J.; Zhu, P.; Liu, X.; Zheng, Z. Unveiling the origin of alkali metal promotion in CO_2 methanation over Ru/ZrO_2. *Appl. Catal. B Environ.* **2022**, *314*, 121476. [CrossRef]
27. Juneau, M.; Vonglis, M.; Hartvigsen, J.; Frost, L.; Bayerl, D.; Dixit, M.; Mpourmpakis, G.; Morse, J.R.; Baldwin, J.W.; Willauer, H.D.; et al. Assessing the viability of K-Mo_2C for reverse water–gas shift scale-up: Molecular to laboratory to pilot scale. *Energy Environ. Sci.* **2020**, *13*, 2524–2539. [CrossRef]
28. Zhang, Q.; Pastor-Pérez, L.; Jin, W.; Gu, S.; Reina, T.R. Understanding the promoter effect of Cu and Cs over highly effective β-Mo_2C catalysts for the reverse water-gas shift reaction. *Appl. Catal. B Environ.* **2019**, *244*, 889–898. [CrossRef]
29. Bugyi, L.; Oszkó, A.; Solymosi, F. Spectroscopic study on the formation of CO^{-2} on K-promoted Mo_2C/Mo(100) surface. *Surf. Sci.* **2000**, *461*, 177–190. [CrossRef]
30. Porosoff, M.D.; Baldwin, J.W.; Peng, X.; Mpourmpakis, G.; Willauer, H.D. Potassium-promoted molybdenum carbide as a highly active and selective catalyst for CO_2 conversion to CO. *ChemSusChem* **2017**, *10*, 2408–2415. [CrossRef]
31. Xu, J.; Gong, X.; Hu, R.; Liu, Z.-W.; Liu, Z.-T. Highly active K-promoted Cu/β-Mo_2C catalysts for reverse water gas shift reaction: Effect of potassium. *Mol. Catal.* **2021**, *516*, 111954. [CrossRef]
32. Ye, X.; Ma, J.; Yu, W.; Pan, X.; Yang, C.; Wang, C.; Liu, Q.; Huang, Y. Construction of bifunctional single-atom catalysts on the optimized β-Mo_2C surface for highly selective hydrogenation of CO_2 into ethanol. *J. Energy Chem.* **2022**, *67*, 184–192. [CrossRef]
33. Kowalik, P.; Próchniak, W.; Borowiecki, T. The effect of alkali metals doping on properties of Cu/ZnO/Al_2O_3 catalyst for water gas shift. *Catal. Today* **2011**, *176*, 144–148. [CrossRef]
34. Delley, B. From molecules to solids with the $DMol^3$ approach. *J. Chem. Phys.* **2000**, *113*, 7756–7764. [CrossRef]
35. Perdew, J.P.; Burke, K.; Ernzerhof, M. Generalized Gradient Approximation Made Simple. *Phys. Rev. Lett.* **1996**, *77*, 3865–3868. [CrossRef]
36. Delley, B. An all-electron numerical method for solving the local density functional for polyatomic molecules. *J. Chem. Phys.* **1990**, *92*, 508–517. [CrossRef]
37. Halgren, T.A.; Lipscomb, W.N. The synchronous-transit method for determining reaction pathways and locating molecular transition states. *Chem. Phys. Lett.* **1977**, *49*, 225–232. [CrossRef]
38. Henkelman, G.; Jónsson, H. Improved tangent estimate in the nudged elastic band method for finding minimum energy paths and saddle points. *J. Chem. Phys.* **2000**, *113*, 9978–9985. [CrossRef]
39. Yang, C.; Guo, K.; Yuan, D.; Cheng, J.; Wang, B. Unraveling Reaction Mechanisms of Mo_2C as Cathode Catalyst in a Li-CO_2 Battery. *J. Am. Chem. Soc.* **2020**, *142*, 6983–6990. [CrossRef]
40. Hammer, B.; Nørskov, J.K. Electronic factors determining the reactivity of metal surfaces. *Surf. Sci.* **1995**, *343*, 211–220. [CrossRef]
41. Mortensen, J.J.; Hammer, B.; Nørskovi, J.K. A theoretical study of adsorbate–adsorbate interactions on Ru(0001). *Surf. Sci.* **1998**, *414*, 315–329. [CrossRef]
42. Günther, S.; Esch, F.; del Turco, M.; Africh, C.; Comelli, G.; Kiskinova, M. K-stabilized high-oxygen-coverage states on Rh(110): A low-pressure pathway to formation of surface oxide. *J. Phys. Chem. B* **2005**, *109*, 11980–11985. [CrossRef] [PubMed]
43. McGuire, N.K.; O'Keeffe, M. Bond lengths in alkali metal oxides. *J. Solid State Chem.* **1984**, *54*, 49–53. [CrossRef]
44. Tai, J.; Ge, Q.; Davis, R.J.; Neurock, M. Adsorption of CO_2 on Model Surfaces of Cesium Oxides Determined from First Principles. *J. Phys. Chem. B* **2004**, *108*, 16798–16805. [CrossRef]

45. Porosoff, M.D.; Yang, X.; Boscoboinik, J.A.; Chen, J.G. Molybdenum carbide as alternative catalysts to precious metals for highly selective reduction of CO_2 to CO. *Angew. Chem. Int. Ed.* **2014**, *53*, 6705–6709. [CrossRef]
46. Porosoff, M.D.; Kattel, S.; Li, W.; Liu, P.; Chen, J.G. Identifying trends and descriptors for selective CO_2 conversion to CO over transition metal carbides. *Chem. Commun.* **2015**, *51*, 6988–6991. [CrossRef]
47. Lee, J.S.; Kim, S.; Kim, Y.G. Electronic and geometric effects of alkali promoters in CO hydrogenation over K/Mo_2C catalysts. *Top. Catal.* **1995**, *2*, 127–140. [CrossRef]
48. Bugyi, L.; Solymosi, F. Effects of Potassium on the Chemisorption of CO on the Mo_2C/Mo(100) Surface. *J. Phys. Chem. B* **2001**, *105*, 4337–4342. [CrossRef]
49. Solymosi, F.; Bugyi, L. Effects of potassium on the chemisorption of CO2 and CO on the Mo_2C/Mo (100) surface. *Catal. Lett.* **2000**, *66*, 227–230. [CrossRef]
50. Hammer, B. Adsorption, diffusion, and dissociation of NO, N and O on flat and stepped Ru(0001). *Surf. Sci.* **2000**, *459*, 323–348. [CrossRef]
51. Wang, Y.-X.; Wang, G.-C. A systematic theoretical study of the water gas shift reaction on the Pt/ZrO_2 interface and Pt(111) face: Key role of a potassium additive. *Catal. Sci. Technol.* **2020**, *10*, 876–892. [CrossRef]
52. Austin, N.; Ye, J.; Mpourmpakis, G. CO_2 activation on Cu-based Zr-decorated nanoparticles. *Catal. Sci. Technol.* **2017**, *7*, 2245–2251. [CrossRef]
53. Freund, H.-J.; Roberts, M.W. Surface chemistry of carbon dioxide. *Surf. Sci. Rep.* **1996**, *25*, 225–273. [CrossRef]
54. Wurth, W.; Stöhr, J.; Feulner, P.; Pan, X.; Bauchspiess, K.R.; Baba, Y.; Hudel, E.; Rocker, G.; Menzel, D. Bonding, structure, and magnetism of physisorbed and chemisorbed O_2 on Pt(111). *Phy. Rev. Lett.* **1990**, *65*, 2426–2429. [CrossRef] [PubMed]
55. Austin, N.; Butina, B.; Mpourmpakis, G. CO_2 activation on bimetallic CuNi nanoparticles. *Prog. Nat. Sci. Mater.* **2016**, *26*, 487–492. [CrossRef]
56. Dixit, M.; Peng, X.; Porosoff, M.D.; Willauer, H.D.; Mpourmpakis, G. Elucidating the role of oxygen coverage in CO_2 reduction on Mo_2C. *Catal. Sci. Technol.* **2017**, *7*, 5521–5529. [CrossRef]